Hub | ScienceDirect | Scopus | SciTopics | Applications Register | Login | Go to SciVal Suite
You have Guest access to ScienceDirec
Find out more...

Home Browse Search My settings My alerts Help

All fields Author Advanced search
Journal/Book title Volume Issue Page Search ScienceDirect Search tips

BIOSENSORS2012
15-18 May 2012 • Cancun, Mexico
21st Anniversary World Congress or Biosensors

Back to results | < Previous 15 of 42 Next > Font Size: A A

PDF (476 K) Export citation

Thumbnails | Full-Size images

Article | Figures/Tables | References

Related Articles

- A jet-cooled infrared spectrum of the formic acid dimer... *Chemical Physics Letters*
- Cavity ring-down spectroscopy of jet-cooled 1-pyrenecar... *Chemical Physics Letters*
- Absorption spectrum of nitrous acid for the [nu]1+2[nu]... *Journal of Quantitative Spectroscopy and Radiative Tran...*
- Investigation on an evanescent wave fiber-optic absorpt... *Optics Communications*
- Cavity ring-down spectroscopy with Fourier-transform-li... *Chemical Physics Letters*

View more related articles

Related reference work articles e.g. encyclopedias

- LASER-BASED TECHNIQUES *Encyclopedia of Analytical Science*

More related reference work articles

VSW SciClick

Free Research Videos
Scroll through our list of videos related to research conducted utilizing Hysitron technology Learn More

Opportunity to be Heard
Seize the opportunity to become a part of a future Hysitron-Elsevier published content now! Learn More

Sensors and Actuators A: Physical
Volume 165, Issue 2, February 2011, Pages 230-238

doi:10.1016/j.sna.2010.11.005 | How to Cite or Link Using DOI
Copyright © 2010 Elsevier B.V. All rights reserved.
Permissions & Reprints

Performance evaluation of a trace-moisture analyzer based on cavity ring-down spectroscopy: Direct comparison with the NMIJ trace-moisture standard

Hisashi Abe[a], , **and Koichi M.T. Yamada**[b] *[Author vitae]*

[a] National Metrology Institute of Japan (NMIJ), AIST, Tsukuba Central 3, Tsukuba 305-8563, Japan

[b] Institute for Environmental Management Technology (EMTech), AIST, Tsukuba-West, Tsukuba 305-8569, Japan

Received 9 August 2010; revised 5 November 2010; accepted 11 November 2010. Available online 19 November 2010.

Abstract

The performance of a moisture analyzer (MA) based on cavity ring-down spectroscopy (CRDS) was evaluated by direct comparison with the primary trace-moisture standard developed at the National Metrology Institute of Japan (NMIJ). The limit of detection for trace moisture in nitrogen gas by the CRDS-based MA, expressed in amount fraction (mole fraction), was estimated to be 1 nmol mol^{-1} or less. The CRDS-based MA showed excellent performance in terms of linearity, accuracy, time response, stability, and reproducibility over four years. It was found for a moderate range of pressures and temperatures that we can measure trace moisture in nitrogen gas with a relative standard uncertainty of approximately 4% down to approximately 10 nmol mol^{-1}, even using a simple CRDS-based MA that measures only the peak intensity of the absorption line, provided that the MA is properly calibrated on the basis of a reliable trace-moisture standard.

Keywords: Diffusion tube; Humidity standard; Measurement performance; Metrological traceability; Sensor test; Standard gas

Article Outline

1. Introduction

2. Experimental

3. Measurement and analytical procedure

4. Results and discussion
   4.1. Limit of detection
   4.2. Pressure effect
   4.3. Temperature effect
   4.4. Linearity
   4.5. Accuracy
   4.6. Time response
   4.7. Stability and reproducibility

5. Conclusions

Acknowledgements

References

Vitae

1. Introduction

Moisture is an extremely troublesome impurity that is difficult to remove from high-purity gases. In the semiconductor industry, residual moisture in process gases is considered to adversely affect the yield and product quality of semiconductor devices even at trace levels below 1 μmol mol^{-1} in amount fraction (mole fraction) [1]. These facts emphasize the importance of the reliable measurement of residual trace moisture in gases. Various measuring instruments for detecting trace moisture in gases are available commercially, and used widely [2] not only at production sites but also in scientific experiments. However, the performance of such instruments in the range below 1 μmol mol^{-1} has hardly been evaluated experimentally in a manner traceable to the International System of Units (SI) owing to the fact that there was no primary trace-moisture standard until only some years ago. The National Metrology Institute of Japan (NMIJ) established the primary trace-moisture standard in 2007 using a diffusion-tube method [3], [4] and [5], with which the performance of some commercially available instruments (two chilled hygrometers and five aluminum oxide capacitive sensors) have been tested preliminarily [6]. It was found that there are problems with all the instruments in terms of accuracy, time response, and stability (measurement repeatability) in the range below 100 nmol mol^{-1}, indicating that it is important to evaluate the performance of measuring instruments for trace moisture on the basis of a primary trace-moisture standard.

In this study, we quantitatively evaluated the measurement performance of a moisture analyzer (MA) based on cavity ring-down spectroscopy (CRDS) [7], [8], [9] and [10], by direct comparison with the NMIJ magnetic suspension balance/diffusion-tube humidity generator (MSB/DTG) which can generate trace moisture in nitrogen gas in the range between 12 nmol mol^{-1} and 1400 nmol mol^{-1}. CRDS has recently been developed to detect trace species although its measurement principle was reported more than two decades ago. In a typical CRDS experiment, an optical cavity consisting of two highly reflective mirrors is used as a sample cell. Laser light is injected into the sample cell through a mirror on one side of the cell and reflected back and forth inside the sample cell by highly reflective mirrors. The light transmitted through the mirror on the other side of the cell is monitored using a photodetector. When the laser is turned off, the transmitted signal begins to decrease by a factor of $\exp(-t/\tau)$, where t is the time and τ is the ring-down time, which is the time constant of the decaying transmitted signal. If there is a species in the sample cell that absorbs the laser light, the transmitted signal decays more rapidly and the ring-down time becomes smaller owing to the absorption. The number density of the species can be determined by analyzing the change in the ring-down time. The use of highly reflective mirrors makes it possible to achieve an extraordinarily long effective path length, on the order of 10 km or more, making CRDS highly sensitive. It is expected to be a powerful and effective tool for measuring trace moisture in gases below 1 μmol mol^{-1}. In this paper, we present and discuss the results of the study in terms of the limit of detection, linearity, accuracy, time response, stability, and reproducibility. The pressure and temperature effects on measurement are also discussed.

2. Experimental

The apparatus used in this study was essentially the same as that described in Ref. [4]. Dry nitrogen (N_2) gas was prepared using a purifier (Saes Getters, Monotorr PS4-MT3-N-1). The mole fraction of residual moisture in the dry gas was estimated to be 1 nmol mol^{-1} or less. The dry gas was introduced into the inlet of the generation chamber and the bypass line using two thermal mass flow controllers (Stec, SEC-F440 M), referred to as MFC1 and MFC2. The total flow rate was controlled using MFC1 in the range between 1 L min^{-1} and 20 L min^{-1} (the flow rates presented in this paper correspond to those measured under the standard conditions of 101.325 kPa and 0 ℃). A portion of the flow, at a flow rate of 0.1 L min^{-1}, was led to the generation chamber using MFC2. The temperature of the chamber was maintained at 25 ℃ or 60 ℃. Inside the chamber, a diffusion cel l [3] was suspended from the measuring load of the MSB (Rubotherm). Water was stored in the diffusion cell, and water vapor that evaporated through the diffusion tube was diluted with the dry N_2 gas flowing from the inlet. Humid gas generated in this manner was taken from the outlet of the chamber. The line from the outlet was connected to the bypass line, and the humid gas was mixed and diluted with the dry N_2 gas. This mixed flow was divided into two: one flow was introduced into a pressure regulator (PR) to control the pressure inside the generation chamber, which was maintained at 155 kPa. The other was led to the CRDS-based MA (Tiger Optics, MTO-1000-H_2O). The temperature of the sample cell of the MA was measured using a platinum resistance thermometer mounted immediately underneath the sample cell. Pressure inside the sample cell was maintained using a manual pressure regulator installed in the MA at P = (135.0 ± 3.1) kPa, (122.1 ± 1.2) kPa, or (103.4 ± 1.1) kPa, where the numbers in parentheses represent the mean ± 2× standard deviation. The pressure measurement was performed in the same manner as that descried in Section 3.
The mole fraction of water, x_w, is given by

(1)

where N is the amount-of-substance of water vapor evaporated per unit time from the diffusion cell, N_b is the amount-of-substance of water vapor adsorbed/desorbed per unit time from the inside surfaces of the generation chamber and tubes used for the pipework, F is the molar flow rate of the dry gas, and x_b is the mole fraction of residual moisture in the dry gas. N was obtained from the measurement of a mass-loss rate of the diffusion cell using the MSB. The MSB is capable of weighing the diffusion cell placed inside the generation chamber using an analytical balance placed outside the generation chamber by adopting a magnetic suspension system. The MSB used in this study is described in detail elsewhere [3]. The mass-loss rate was calculated from the mass and time data using least-squares fitting with a linear function. The mass data were obtained by measuring the mass of the diffusion cell every 12 min using the MSB. The adjustment of the indication of the MSB to zero and the calibration of the MSB were performed at each mass measurement. Internal weights of the analytical balance in the MSB were used for the calibration. These weights were calibrated against external weights in advance. The buoyancy effect on the mass data was compensated for in the same manner as that described in Ref. [4]. The time at each mass measurement was recorded using the internal clock of a personal computer synchronized every 60 min to the Network Time Protocol (NTP) server at the National Institute of Advanced Industrial Science and Technology (AIST). The accuracy of the time interval measured using this clock was verified beforehand by simultaneously counting the number of pulses generated at a frequency of 10 kHz using a function generator (Iwatsu, SG-4115). F was measured using mass flow meters (MFMs)

composed of critical flow Venturi nozzles [11], [12] and [13] or MFC1 calibrated against the MFMs. The external weights, function generator, and MFMs were calibrated in advance utilizing the Japan Calibration Service System (JCSS) [14], through which the metrological traceability of the measurement to the SI was guaranteed.

3. Measurement and analytical procedure

The mole fraction x_w was varied in the range between 12 nmol mol^{-1} and 1400 nmol mol^{-1} by adjusting the flow rate of the dry gas through the bypass line and by maintaining the temperature of the chamber at 25 ℃ or 60 ℃. The uncertainty of the standard value of x_w is summarized in Table 1. Keeping x_w constant in the range mentioned above, near-infrared spectra were recorded using a built-in function of the MA, which varies the temperature of the laser diode of the MA, t_{LD}, to scan the laser frequency. Using this function, the ring-down time of the cavity of the MA containing the trace moisture, τ, was measured as a function of t_{LD}, as shown in Fig. 1(a). For reference, the ring-down time of the cavity containing only the dry gas, τ_0, was also measured, as shown in Fig. 1(b). In Fig. 1(b), data were fitted using least-squares fitting with a cubic function; this cubic function provided τ_0 in this study. The lack of a discernible peak in Fig. 1(b) indicates that the amount of the background moisture is lower than the limit of detection of the MA, which is estimated to be 1 nmol mol^{-1} or less in Section 4.1.

Table 1. Uncertainty of the trace moisture standard used in the present study.[a]

Standard value	12.00	70.0	150.00	300.0	5
Uncertainty component					
• Evaporation rate	0.172	1.004	0.575	1.150	2.
• Adsorbed/desorbed moisture	0.014	0.084	0.031	0.062	0.
• Flow rate of dry gas	0.024	0.139	0.297	0.595	1.
• Residual moisture in zero gas	0.360	0.360	0.360	0.360	0.
Combined standard uncertainty	0.40	1.1	0.75	1.4	2.
Relative combined standard uncertainty [%]	3.3	1.5	0.50	0.47	0.

[a]All entries are given in nmol mol^{-1} unit (except relative combined standard uncertainty).

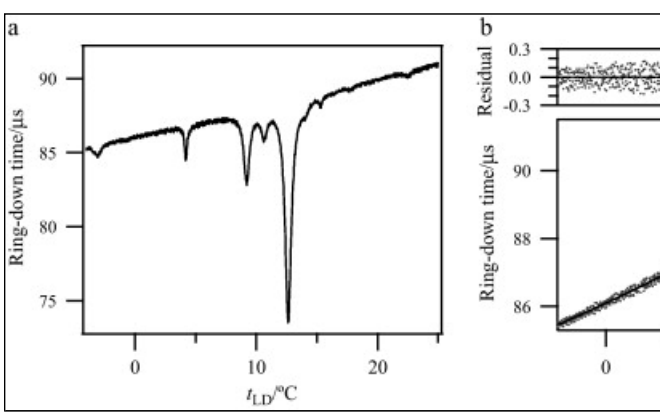

Fig. 1.

The observed ring-down time for the cavity of the MA containing trace moisture (a), and that for the cavity of the MA containing only dry gas (b),

are presented as functions of the temperature of the laser diode. In (b), the best fit curve obtained using the least-squares fitting with a cubic function and residuals from the fit are also shown.

The absorption coefficient of water, α, was obtained using

$$\alpha = \frac{1}{c}\left(\frac{1}{\tau} - \frac{1}{\tau_0}\right), \qquad (2)$$

where c is the speed of light in the medium within the cavity and can be approximated to be the same as that in vacuum in this study. Fig. 2(a) shows α as a function of t_{LD}. Peaks in the figure are attributable to the rotation–vibration transitions of water, and their center positions expressed in ℃ were obtained using least-squares fitting with Lorentzian functions. Comparing these line positions with the corresponding values of wavenumber (≡v/c where v is the frequency) reported in the HITRAN2008 database [15], the temperature scales were converted into the wavenumber scales (in cm^{-1}). Thus, the near-infrared spectra of water, that is, α as a function of wavenumber, were obtained, as shown in Fig. 2(b). The spectra were fitted again using least-squares fitting (line shape fit) with Lorentzian functions in the range between approximately 7175 cm^{-1} and 7188 cm^{-1} to obtain the amplitude a, the center position v_0, and the Lorentz half width b_L (half width at half maximum, HWHM) to reproduce the spectra using the formula:

$$\alpha(v) = a_0 + \sum_i \alpha_i(v) = a_0 + \sum_{i=1} \frac{a_i}{[(v - v_{0i})^2 + b_{L,i}^2]}, \qquad (3)$$

where a_0 represents the baseline offset and the subscript i refers to the ith line. In this study, we have focused only on the strongest peak at 7181.16 cm^{-1}, that is, $2_{02} \leftarrow 3_{03}$ transition of $v_1 + v_3$ band, as denoted by the asterisk in Fig. 2(b). The absorption coefficient of this line obtained from the least-squares analysis described above is rewritten here as $\alpha(v) = a/[(v - v_0)^2 + b_L^2]$. The pressure inside the sample cell P was calculated from b_L using

$$b_L = \gamma(T)P, \qquad (4)$$

where $\gamma(T)$ is the broadening coefficient (HWHM) of H_2O by N_2 at a temperature T. The pressure broadening due to H_2O–H_2O collisions can be ignored because, in this study, the water concentration is extremely low. $\gamma(T)$ is expressed as

$$\gamma(T) = \gamma_0\left(\frac{T_0}{T}\right)^n, \qquad (5)$$

where γ_0 is the coefficient at T_0. For the $2_{02} \leftarrow 3_{03}$ line, n = 0.73 [15] and [16] and $\gamma_0 = 1.118 \times 10^{-6}$ cm^{-1}/Pa at T_0 = 296 K [17] were used to derive P.

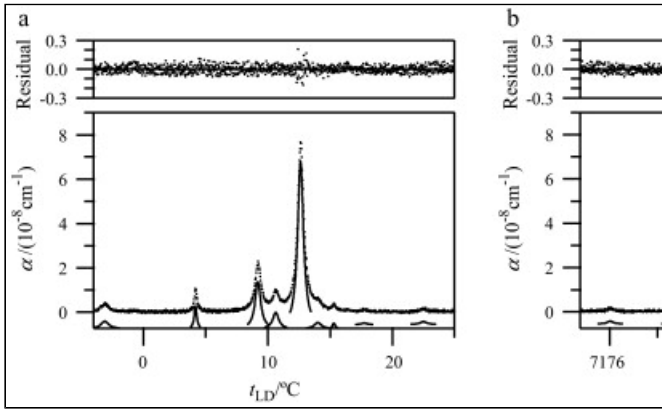

Fig. 2.

The absorption coefficient of water recorded as a function of the temperature of the laser diode (a) is converted to the spectrum with the wavenumber scale as shown in (b). The spectra were fitted with Lorentzian functions (solid lines) and residuals obtained from the fit are plotted.

The line width (HWHM) of the diode laser of the MA ($\sim 3 \times 10^{-5}$ cm^{-1}) was much smaller than that of the absorption line in this study (>0.1 cm^{-1}), thus confirming that the effect of the line width of the diode laser on the spectral line shape can be ignored in the present study.

4. Results and discussion

4.1. Limit of detection

Fig. 3(a) shows the spectra recorded with x_w = 12 nmol mol^{-1} and P = 135 kPa, 122 kPa, and 103 kPa, respectively. The spectra were fitted with Lorentzian functions (solid lines), and residuals obtained from the fit are plotted in Fig. 3(b). The line profiles obtained from the fit are offset downward for visibility. Neither significant systematic deviations nor fringe structures due to optical interference were observed in the residuals. The absorption coefficient at the peak (the line center) position of the $2_{02} \leftarrow 3_{03}$ transition and the standard deviation of the residuals at each of the three pressures are approximately 1.2×10^{-8} cm^{-1} and 3.7×10^{-10} cm^{-1}, respectively. The baseline offset a_0 in this study was 2.2×10^{-12} cm^{-1}, and its contribution to the limit of detection could be ignored. If we adopt 3× standard deviation as the limit of detection [18] and [19], it corresponds to x_w = 1.1 nmol mol^{-1}.

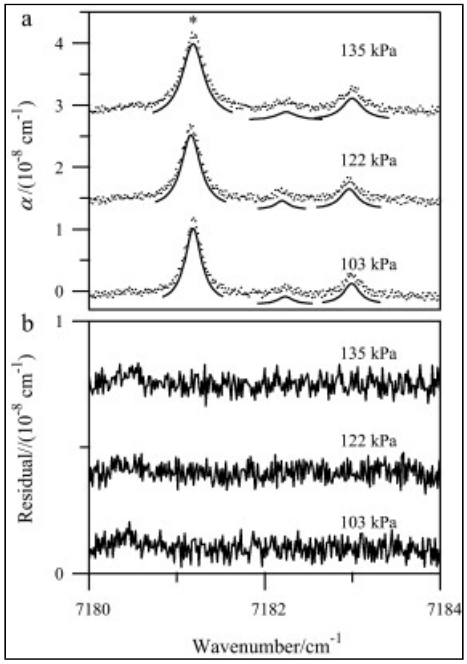

Fig. 3.

Infrared spectra of water recorded with x_w = 12 nmol mol^{-1} at pressures of 135 kPa, 122 kPa, and 103 kPa are shown in (a). Asterisk indicates absorption line analyzed in the present study. The spectra were fitted with Lorentzian functions (solid lines) and residuals obtained from the fit are plotted in (b).

The minimum measurable absorption coefficient α_{min} can be estimated using [10]

$$\alpha_{min} = \frac{1}{c\tau_0}\frac{\Delta\tau_{min}}{\tau_0}, \qquad (6)$$

where $\Delta\tau_{min}$ is the minimum detectable change in the cavity ring-down time. The numerical values of τ_0 and the standard deviation of the residuals obtained from the fit of the data shown in Fig. 1(b) are 88.44 μs and 0.08 μs, respectively. If we adopt 3× standard deviation as $\Delta\tau_{min}$ in Eq. (6), α_{min} is estimated to be 1.0 × 10^{-9} cm^{-1}, which corresponds to x_w = 1.0 nmol mol^{-1} and is consistent with the limit of detection estimated above. If we adopt $\sqrt{2}\times$ standard deviation as $\Delta\tau_{min}$ [20], [21] and [22], α_{min} corresponds to x_w = 0.48 nmol mol^{-1}, which is consistent with x_w = 0.44 nmol mol^{-1} reported in Ref. [22], where the same type of a commercially available MA was used.

4.2. Pressure effect

Fig. 3(a) also demonstrates that the absorption coefficient at the peak of the line $\alpha(\nu_0)$ does not depend on the pressure inside the sample cell, as pointed out by Dudek et al. [23]. This can be explained as follows. $\alpha(\nu)$ is related to the number density of water, N_w, and the net absorption cross section $\sigma(\nu)$ by

$$\alpha(\nu)=N_w\sigma(\nu).$$

When the spectral line shape can be approximated by a Lorentzian function because the pressure inside the sample cell P is sufficiently high, the net

absorption cross section at the center position, $\sigma(\nu_0)$, is given by [24]

$$\sigma(\nu_0) = \frac{S(T)}{\pi\gamma(T)P}, \qquad (8)$$

where $S(T)$ is the line strength at T. The number density, N_w, is given by

$$N_w = x_w N_g = \frac{x_w P}{kT}, \qquad (9)$$

where N_g and k represent the number density of total gas and the Boltzmann constant, respectively. Using Eqs. (7), (8) and (9), we obtain

$$\alpha(\nu_0) = \frac{S(T)x_w}{\pi\gamma(T)kT}, \qquad (10)$$

which is independent of P. From Eqs. (2) and (10), x_w is given by

$$x_w = \frac{\pi\gamma(T)kT}{cS(T)}\left(\frac{1}{\tau(\nu_0)} - \frac{1}{\tau_0(\nu_0)}\right), \qquad (11)$$

which is also independent of P. Eq. (11) indicates that x_w can be determined directly from the measurement of $\tau(\nu_0)$, $\tau_0(\nu_0)$, and T without using an analytical curve (calibration curve), if the line shape can be approximated by a Lorentzian function and $\gamma(T)$ and $S(T)$ are known.

However, Eq. (11) is not applicable when P is low because the line shape deviates from the Lorentzian function. In order to estimate the pressure effect on the measurement of x_w in the low-P region, we assume here that the line shape can be expressed using a Voigt function in the low-P region. $\sigma(\nu_0)$ is given by [24]

$$\sigma(\nu_0) = S(T)D\frac{A}{\pi}\int_{-\infty}^{\infty}\frac{e^{-y^2}}{A^2+y^2}dy \equiv S(T)DK(A), \qquad (12)$$

where

$$A = \left(\frac{b_L}{b_D}\right)\sqrt{\ln 2} = \left[\frac{\gamma(T)P}{b_D}\right]\sqrt{\ln 2} \qquad (13)$$

$$D = \left(\frac{1}{b_D}\right)\sqrt{\frac{\ln 2}{\pi}}, \qquad (14)$$

and b_D is the Doppler half-width (HWHM). The numerical value of b_D can be calculated using

$$b_D = 3.581 \times 10^{-7}\nu_0\sqrt{\frac{T}{M}}, \qquad (15)$$

where M is the molecular mass of the absorbing gas (18.02 g mol^{-1} for H_2O). Using Eqs. (2), (7) and (9), and (12), (13) and (14), x_w is given by

(16)

$$x_w = \frac{kT}{cS(T)PDK(A)}\left(\frac{1}{\tau(\nu_0)} - \frac{1}{\tau_0(\nu_0)}\right)$$
$$= \frac{b_D^2(T)\sqrt{\pi^3}kT}{cS(T)\gamma(T)P^2(\ln 2)}\left(\frac{1}{\tau(\nu_0)} - \frac{1}{\tau_0(\nu_0)}\right)$$
$$\times\left[\int_{-\infty}^{\infty}\frac{e^{-y^2}}{(\ln 2)[\gamma(T)P/b_D(T)]^2 + y^2}dy\right]^{-1},$$

which depends on P in contrast to Eq. (11), indicating the necessity of measuring P to determine x_w. The ratio of x_w calculated using Eq. (11) to that calculated using Eq. (16) is thus given by

$$\frac{(x_w)_{\mathrm{Eq.(11)}}}{(x_w)_{\mathrm{Eq.\ (16)}}} = \pi\gamma(T)PDK(A). \tag{17}$$

The function $K(A)$ can be calculated using [24]

$$K(A)=\exp(A^2)\mathrm{erfc}(A), \tag{18}$$

where erfc(A) is the complementary error function. The ratio calculated using Eqs. (13), (14), (15) and (17), and (18) in the range down to 30 kPa is shown in Fig. 4 as indicated by the solid line. Open circles in the figure denote the values calculated from experimental data, where error bars represent the expanded uncertainty with a coverage factor of 2 (≈ 95% level of confidence). The figure indicates that x_w is underestimated if Eq. (11) is used to determine x_w in the low-P region.

Fig. 4.

The ratio of x_w calculated on the basis of the Lorentzian function to that calculated on the basis of the Voigt function is shown as a function of the pressure inside the sample cell (solid line). Open circles denote the values calculated from experimental data, where error bars represent the expanded uncertainty with a coverage factor of 2 (≈95% level of confidence).

It should be noted that line shape functions other than the Voigt function are proposed to more accurately reproduce the line shape of this absorption line

at pressures below 30 kPa [17], and those line shape functions are required to accurately analyze the data at lower pressures.

4.3. Temperature effect

Eq. (11) also indicates that the measurement can be affected by temperature. $S(T)$ is related to the strength S_0 at a reference temperature T_0 by [25]

$$S(T) = S_0 \left(\frac{T_0}{T}\right)^{1.5} \exp\left[-\frac{hcE_0}{k}\left(\frac{1}{T} - \frac{1}{T_0}\right)\right], \tag{19}$$

where h is the Planck constant and E_0 is the energy of the lower level of the transition (136.76 cm^{-1} for this transition [15] and [16]). The numerical value of S_0 at T_0 = 296 K for this transition was reported to be 1.5048×10^{-20} cm molecule^{-1} [17]. The value of $\partial x_w/\partial T$ is calculated, using Eqs. (5) and (11), and (19), to be positive for T > 112 K. This implies that, in measurement near room temperature, the underestimation of T leads to the underestimation of x_w, which was observed in a previous study [4]. The calculation of $(\partial x_w/\partial T)/x_w$ in the case of τ = 80.00 μs and τ_0 = 88.44 μs predicted that the relative standard uncertainty in the measurement of x_w due to the temperature effect would become 0.37% at approximately 296 K if the standard uncertainty of T in Eq. (11) is 1 K.

4.4. Linearity

Fig. 5(a) shows $\alpha(\nu_0)$ as a function of x_w in the range between 12 nmol mol^{-1} and 1400 nmol mol^{-1} measured at approximately 135 kPa, 122 kPa, and 103 kPa. The peak intensity $\alpha(\nu_0)$ was simply taken from the largest value of $\alpha(\nu)$ in the spectral range between 7175 cm^{-1} and 7188 cm^{-1} (the value obtained from the least-squares analysis was not used). Each set of data was analyzed by weighted least-squares fitting with a linear function, where the reciprocal of the squared uncertainty of the peak intensity, $1/u^2(\alpha)$, was used for the weight. $u(\alpha)$ was estimated from the standard deviation of the residuals near the peak obtained from the least-squares fitting described in Section 3. The result of the fitting shows that the slopes of the lines are nearly independent of P, as expected from Eq. (10), the difference in slopes being less than 2.3%. The integrated line intensities for the strongest absorption line, $\mathcal{A} = \int \alpha(\nu)d\nu$, were obtained by least-squares fitting using Eq. (3). $\mathcal{A}$ is shown as a function of x_w for the three measured pressures in Fig. 5(b). Each set of data was also analyzed by weighted least-squares fitting with a linear function, where the reciprocal of the squared uncertainty of the integrated line intensity, $1/u^2(\mathcal{A})$, was used for the weight. The uncertainty obtained from the line shape fit described in Section 3 was used for $u(\mathcal{A})$. The slopes depend on P, in contrast to the case of $\alpha(\nu_0)$.

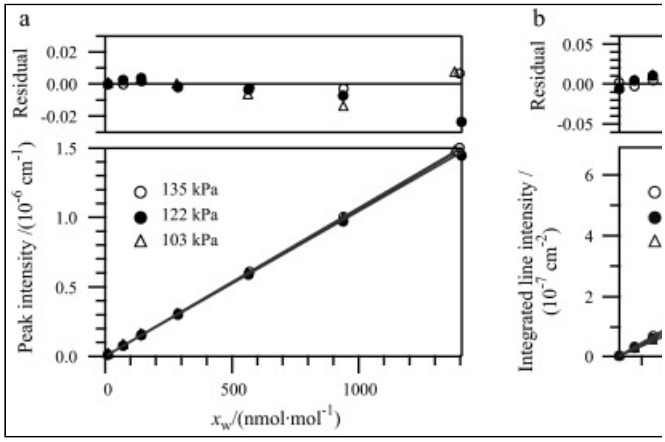

Fig. 5.

The effects of the gas pressure on the absorption intensity observed at P = 135 kPa, 122 kPa, and 103 kPa are shown: (a) peak intensity and (b) integrated line intensity. The data were fitted using least-squares analysis with linear functions (solid lines). The residuals obtained from the analysis are also shown in the top.

The values of the reduced (normalized) chi-square, χ_r^2, obtained from the fits with linear functions for five degrees of freedom are summarized in Table 2. In the case of the peak intensity, the values are close to 1, indicating that the observed data can be explained by the linear functions. In contrast, in the case of the integrated line intensity, the values are much larger than 1. This is probably attributable to the underestimation of $u({}_{\nu}\mathcal{A})$. The uncertainty obtained from the line shape fit does not include the uncertainty due to the error in the cubic function that provides τ_0, the insufficient knowledge of the line shape, and the fluctuation of the laser frequency at each measurement point. Careful analysis of these effects on $u({}_{\nu}\mathcal{A})$ is important for accurately evaluating the uncertainty of the line strength $u(S_0)$. This is, however, of no immediate relevance to the main subject of the present study, and we do not further discuss this issue in this paper.

Table 2. The χ_r^2 obtained from the fit.

***P*/kPa**	**135**	**122**	**103**
Peak intensity	0.31	2.03	0.70
Integrated line intensity	24.96	63.51	7.02

The CRDS-based MA used in this study is designed to measure only the peak intensity of the absorption line to determine x_w, which has been proved by the present study to be a simple and effective way of maintaining good linearity.

4.5. Accuracy

The accuracy in the measurement of trace moisture using the CRDS-based MA depends on the validity of Eq. (11) and measurement performance of the MA. In order to check the validity and measurement performance, it may be useful to calculate the line strength using Eqs. (5) and (11) with the data obtained in this study, and compare it with that reported in the literature. The

line strengths S_0 at T_0 = 296 K calculated using Eqs. (5) and (11), and (19) are shown as filled circles in Fig. 6. The mean and standard deviation are 1.547×10^{-20} cm molecule^{-1} and 3.5×10^{-22} cm molecule^{-1}, respectively. The mean differs by 2.7% from 1.5048×10^{-20} cm molecule^{-1} reported recently by Lisak et al. [17], also shown as the solid line in Fig. 6. In Ref. [17], the experiments were performed using a primary humidity standard at the National Institute of Standards and Technology (NIST). In addition, Lisak et al. adopted frequency-stabilized cavity ring-down spectroscopy [26] and [27], which enabled them to obtain the high-quality spectra used for the analysis of line strength. Moreover, in their analysis, line profiles more sophisticated than the Lorentzian function were used, and thus they succeeded in obtaining the line strength with a relative standard uncertainty of 0.41%. It is interesting to note that the difference was only 2.7%, as already stated above, although the system used for recording the spectra and the method for analyzing data in this study were much simpler than those described in Ref. [17]. Furthermore, with two exceptions in the low-x_w region, where the uncertainty of the measurement is expected to be large, all the values are positively biased against the value reported in Ref. [17], as shown in Fig. 6, implying that this bias can be compensated for simply by calibrating the MA. After the calibration, the uncertainty of the indication of the MA will be given by combining the uncertainty derived from the standard used for the calibration and that derived from the characteristics of the MA. The former was less than or equal to 3.3%, as shown in Table 1, and the latter may be estimated from the relative standard deviation of the indication of the MA that was approximately less than 2.5%. Therefore, the relative combined uncertainty of the MA after calibration can be estimated to be less than 4.2%.

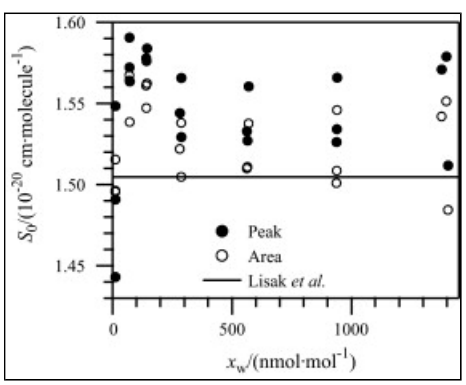

Fig. 6.

The line strengths calculated from the present data are plotted as a function of x_w. Filled circles and open circles denote the line strengths obtained from the peak intensity and the integrated line intensity, respectively. The solid line is the line strength reported by Lisak et al. [17].

Line strength can also be calculated from $\mathcal{A}$ using

(20)

The values obtained using Eq. (20) are recalculated using Eq. (19) to obtain

S_0 at T_0 = 296 K, which are also shown as open circles in Fig. 6 for comparison. The mean and standard deviation are 1.529×10^{-20} cm molecule^{-1} and 2.6×10^{-22} cm molecule^{-1}, respectively. The mean differs by 1.6% from the value reported in Ref. [17].

4.6. Time response

Fig. 7 shows the time response of the indication of the MA based on the Eq. (11) to the changes of x_w in the range between 12 nmol mol^{-1} and 93 nmol mol^{-1}, where the black and gray solid lines represent the standard value and the indication of the MA, respectively. The difference between the two values was discussed in Ref. [4] in terms of the uncertainty of line strength and the temperature effect. The changes were achieved by varying the flow rate of the dry gas. As can be seen in the figure, the response is quite fast. This fast response of the MA should be emphasized because time response is a crucial factor for the performance of trace-moisture analyzers; it has recently been found that some commercially available and conventionally used instruments (chilled mirror hygrometers and aluminum oxide capacitive sensors) show extremely slow or almost no response to the change in the trace-moisture concentration of approximately 100 nmol mol^{-1} or less in a time scale of 5 h [6], although the measurement ranges specified in their catalogs include that region.

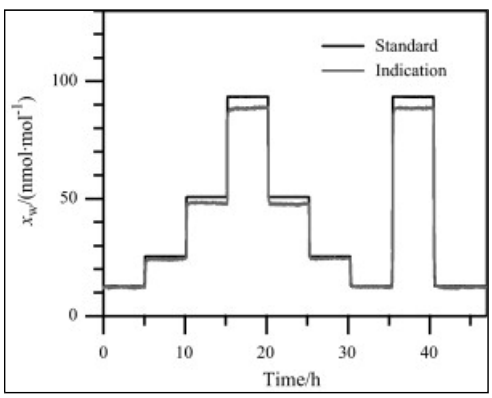

Fig. 7.

The time response of the indication of the CRDS-based MA to the changes in x_w in the range between 12 nmol mol^{-1} and 93 nmol mol^{-1} is shown. The black and gray solid lines represent the standard value and indication of the MA, respectively.

In CRDS, the time needed for a single measurement of ring-down time is very short, which is typically less than a few hundreds of microseconds. Therefore, the time response of a CRDS-based MA is considered to be mainly governed by the time needed for the displacement of the trace-moisture gas in the sample cell. This depends on the flow rate of the gas, the region of x_w measured, the size, structure, and materials of the cell, and how the inner surface of the cell is polished. In the experiment shown in Fig. 7, the flow rate of the gas passing through the sample cell of the MA was 1.0 L min^{-1}. The sample cell is mainly made of electropolished 316L stainless steel with a diameter and a length of approximately 3 cm and 50 cm, respectively. In Fig. 7, the 90% upward and downward response

times between 12 nmol mol^{-1} and 93 nmol mol^{-1} were estimated to be less than 8 min.

4.7. Stability and reproducibility

Fig. 8 shows the time development of the indication recorded for more than 20 h, where the black and gray solid lines represent the standard value and the indication of the MA, respectively. In this experiment, the standard value was maintained at 12.5 nmol mol^{-1}. The mean and standard deviation of the indication were 12.8 nmol mol^{-1} and 0.3 nmol mol^{-1}, respectively. The standard deviation represents the combined uncertainty of the stability (measurement repeatability) of the indication of the MA and the fluctuation of the trace moisture. Eq. (11) indicates that the stability of the indication depends on how precisely $\tau(\nu_0)$ can be measured if the temperature effect is ignorable. This is mainly attributable to the following two factors. One is how precisely the frequency of the laser can be controlled to the center position ν_0. Frequency control is achieved by maintaining the temperature of the laser diode and current. The control method is not particularly precise, and it is possible that small detuning from ν_0 occurs. However, the effect of the detuning on the measurement of $\tau(\nu_0)$ is expected to be small because the absorption line has a relatively broad feature owing to the high pressure inside the sample cell in this study. The other is the uncertainty of measuring $\tau(\nu_0)$. In the low-x_w region where $\tau(\nu_0)$ does not differ greatly from $\tau_0(\nu_0)$, this uncertainty can be approximated by the uncertainty of $\tau_0(\nu_0)$, which was 0.08 μs in this study. This value corresponds to 0.3 nmol mol^{-1} at x_w = 12.8 nmol mol^{-1}, which is comparable to the standard deviation mentioned above. Therefore, the stability observed in Fig. 8 is considered to be limited by this uncertainty. This also means that the uncertainty due to the fluctuation of trace moisture, produced by adsorbed/desorbed moisture and instability in the evaporation, is less than 0.3 nmol mol^{-1} at x_w = 12.8 nmol mol^{-1}. This is consistent with the uncertainty analysis of the standard value shown in Table 1. In the high-x_w region, as the absorption becomes strong, the transmitted signal becomes weak. This reduces the signal-to-noise ratio of the $\tau(\nu_0)$ measurement and begins to increase the uncertainty. The uncertainty depends on the region of x_w measured and the absorption line used to determine x_w in Eq. (11). It is large when a strong absorption line is used in the high-x_w region. Fig. 9 shows the standard deviations of the indications of the MA obtained experimentally, where the black and gray solid lines represent the standard deviations in the cases that the $2_{02} \leftarrow 3_{03}$ transition (S_0 = 1.5048 × 10^{-20} cm molecule^{-1}) and the $2_{12} \leftarrow 3_{13}$ transition (S_0 = 3.772 × 10^{-21} cm molecule^{-1} [17]) of $\nu_1 + \nu_3$ band, respectively, were used to determine x_w. The figure clearly shows that a suitable choice of the absorption line is necessary to reduce the uncertainty.

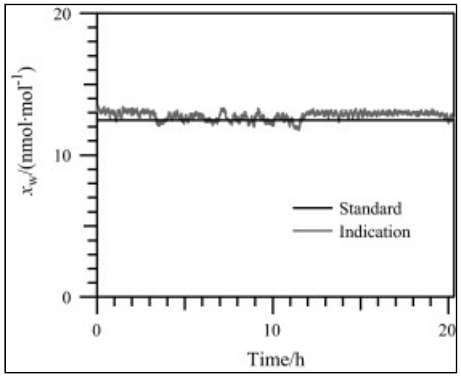

Fig. 8.

The time development of the indication of the MA recorded for more than 20 h is shown, where the black and gray solid lines represent the standard value and indication of the MA, respectively. The standard value was maintained at 12.5 nmol mol^{-1}.

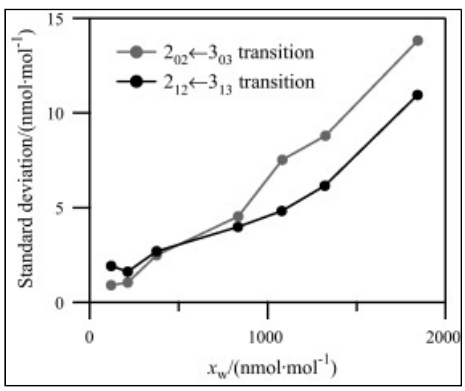

Fig. 9.

The standard deviations of the indications of the MA obtained experimentally are shown. The black line and represents the standard deviations in the cases that the $2_{02} \leftarrow 3_{03}$ transition (S_0 = 1.5048 × 10^{-20} cm molecule^{-1}) of $\nu_1 + \nu_3$ band is used to determine x_w, whereas the gray line represents those for the $2_{12} \leftarrow 3_{13}$ transition (S_0 = 3.772 × 10^{-21} cm molecule^{-1}).

Fig. 10 shows the relative differences between the indications and standard values, where the closed triangles, open circles, and open squares denote those observed in 2006 [4], 2009, and 2010, respectively. The relative difference is defined here by [(standard value-indication)/standard value] × 100. The changes in the relative differences in the four years in the range smaller than 20 nmol mol^{-1} and larger than 50 nmol mol^{-1} are within 4.2% and 1.7%, respectively, demonstrating excellent measurement reproducibility of the CRDS-based MA. The comparatively large changes in the low-x_w region can be explained by 2× relative combined standard

uncertainty of the indications and standard values (≈95% level of confidence), which increases with decreasing x_w. Eq. (11) indicates that the measurement reproducibility depends on how accurately $1/\tau(\nu_0) - 1/\tau_0(\nu_0)$ can always be determined if the temperature effect can be ignored. This is mainly attributable to the following two factors: one is how accurately the frequency of the laser can always be controlled to ν_0. For a short-term duration, the frequency of a laser can be fixed to ν_0 by maintaining temperature and current at appropriate values, as explained above. However, in a long-term duration, it changes slightly with time even if the temperature and current are maintained at those values. This can be considered as the effect of time on the characteristics of the laser diode. Because of this effect, the frequency of the laser deviates gradually from ν_0 as time passes, leading to the underestimation of x_w. We found for the MA used in this study that this effect caused the underestimation to be 14% and 46% for 7 months and 15 months, respectively. A built-in function that compensates for this effect was introduced in the MA. This function periodically scans the frequency of the laser by varying current to find the peak position, and then adjusts current so that the frequency of the laser is controlled to ν_0. This function is indispensable for achieving measurement reproducibility for a long-term duration. The other factor is responsible for the reproducibility of $\tau_0(\nu_0)$, which is given by

$$\tau_0(\nu_0) = \frac{l}{c|1 - R(\nu_0)|}, \qquad (21)$$

where l and $R(\nu_0)$ are the length of the cavity and the reflectivity of the mirror at ν_0, respectively. The ring-down time $\tau_0(\nu_0)$ depends on $R(\nu_0)$ which may change with time owing to, for instance, surface contamination. In this study, we recorded $\tau_0(\nu_0)$ for six months to evaluate this effect, and observed no significant change in $\tau_0(\nu_0)$. The standard deviation of $\tau_0(\nu_0)$ over the six month was 0.12 μs, corresponding to 0.4 nmol mol^{-1} at x_w = 12 nmol mol^{-1}. This good reproducibility of $\tau_0(\nu_0)$ is probably attributable to the fact that the sample gas used in the experiments was high-purity nitrogen including trace moisture less than 2 μmol mol^{-1}, and that the mirrors were not contaminated because they were placed in the sample cell filled with the high-purity nitrogen. It should be noted that even if $R(\nu_0)$ changed for some reason, its effect on the measurement of x_w can be compensated for by measuring $\tau_0(\nu_0)$ again and setting it to a new $\tau_0(\nu_0)$ in Eq. (11), although the limit of detection may be lowered.

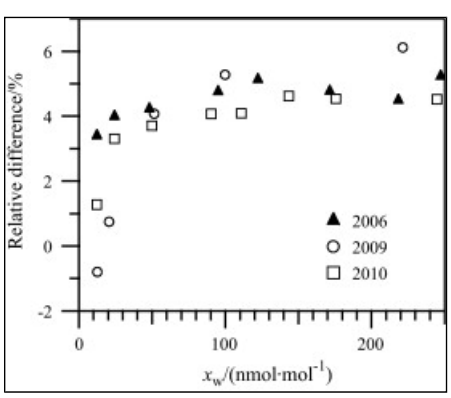

Fig. 10.

The differences between the indications and the standard values are

shown as relative values, where the closed triangles, open circles, and open squares denote the relative differences observed in 2006 [4], 2009, and 2010, respectively. Relative difference is defined by [(standard value-indication)/standard value] × 100.

5. Conclusions

In this study, we have evaluated the measurement performance of a CRDS-based MA by direct comparison with the NMIJ trace-moisture standard. The limit of detection of the MA used in this study was demonstrated to be approximately 1 nmol mol^{-1} or less. The MA showed excellent performance in terms of linearity, time response, stability, and reproducibility even in the region below 1 μmol mol^{-1} where it is not straightforward to measure trace moisture using conventional instruments such as chilled mirror hygrometers and aluminum oxide capacitive sensors. The MA can measure x_w without using an analytical curve in contrast to other instruments such as an atmospheric pressure ionization mass spectrometer (APIMS). Furthermore, it should be emphasized that the CRDS-based MA does not suffer from the atmospheric moisture outside the sample cell because it measures the time of ring-down that occurs inside the sample cell. This is a distinct advantage of the use of the CRDS-based MA over other spectroscopic methods such as tunable diode laser absorption spectroscopy (TDLAS) and Fourier transform infrared (FTIR) spectroscopy, especially for measurements in the trace-moisture region where stray moisture from the atmosphere can be a major source of measurement uncertainty. Moreover, in CRDS, the principle of measurement is on the basis of clear physics, and therefore, the pressure and temperature effects on measurement results can be understood theoretically and quantitatively, as shown in this study. These facts suggest that CRDS is the most reliable method, thus far, for measuring trace moisture in nitrogen gas. Note that the CRDS-based MA can measure trace moisture in gases other than nitrogen as long as the $\gamma(T)$ between the gases and water is known unless the absorption or scattering of the gases lies in the same frequency region as the absorption line of water. It is desirable to evaluate the performance of the CRDS-based MA in other gases by direct comparison with a primary trace-moisture standard. The result of this study also shows that measurement accuracy can be maintained within a relative standard uncertainty of approximately 4% down to approximately 10 nmol mol^{-1} even using a simple CRDS-based MA that measures only the peak value of the absorption line, namely, $\alpha(\nu_0)$, provided that the MA is properly calibrated on the basis of a reliable trace-moisture standard.

Acknowledgements

We would like to thank Dr. Roman Ciuryło and Dr. Daniel Lisak of Uniwersytet Mikołaja Kopernika for helpful comments on the analysis of line shapes and Mr. Hiroshi Kitano of NMIJ for critically reading the manuscript.

References

[1] International Technology Roadmap for Semiconductors. http://www.itrs.net/.

[2] H.H. Funke, B.L. Grissom, C.E. McGrew and M.W. Raynor, Techniques for the measurement of trace moisture in high-purity electronic specialty gases, *Rev. Sci. Instrum.* **74** (2003), pp. 3909–3933. View Record in Scopus | Cited By in Scopus (20)

[3] H. Abe and H. Kitano, Development of humidity standard in trace-moisture

region: characteristics of humidity generation of diffusion tube humidity generator, *Sens. Actuat. A* **128** (2006), pp. 202–208. Abstract | **Article** | PDF (281 K) | View Record in Scopus | Cited By in Scopus (5)

[4] H. Abe and H. Kitano, Improvement of flow and pressure controls in diffusion-tube humidity generator: Performance evaluation trace-moisture generation using cavity ring-down spectroscopy, *Sens. Actuat. A* **136** (2007), pp. 723–729. Abstract | **Article** | PDF (353 K) | View Record in Scopus | Cited By in Scopus (4)

[5] H. Abe, H. Tanaka and H. Kitano, Uncertainty analysis of evaporation rate in magnetic suspension balance/diffusion-tube humidity generator, *Int. J. Thermophys.* **29** (2008), pp. 1555–1566. View Record in Scopus | Cited By in Scopus (1)

[6] H. Abe, A marked improvement in the reliability of the measurement of trace moisture in gases, *Synthesiology* **2** (2009), pp. 206–220. View Record in Scopus | Cited By in Scopus (0)

[7] A. O'Keefe and D.A.G. Deacon, Cavity ring-down optical spectrometer for absorption measurements using pulsed laser sources, *Rev. Sci. Instrum.* **59** (1988), pp. 2544–2551.

[8] D. Romanini and K.K. Lehmann, Ring-down cavity absorption spectroscopy of the very weak HCN overtone bands with six, seven, and eight stretching quanta, *J. Chem. Phys.* **99** (1993), pp. 6287–6301.

[9] G. Berden, R. Peeters and G. Meijer, Cavity ring-down spectroscopy: experimental schemes and applications, *Int. Rev. Phys. Chem.* **19** (2000), pp. 565–607. View Record in Scopus | Cited By in Scopus (395)

[10] M. Mazurenka, A.J. Orr-Ewing, R. Peverall and G.A.D. Ritchie, Cavity ring-down and cavity enhanced spectroscopy using diode lasers, *Annu. Rep. Prog. Chem., Sect. C* **101** (2005), pp. 100–142. View Record in Scopus | Cited By in Scopus (71)

[11] S. Nakao, Y. Yokoi and M. Takamoto, Development of a calibration facility for small mass flow rates of gas and the uncertainty of a sonic venturi transfer standard, *Flow Meas. Instrum.* **7** (1996), pp. 77–83. Abstract | **Article** | PDF (598 K) | View Record in Scopus | Cited By in Scopus (14)

[12] N. Bignell, Using small sonic nozzles as secondary flow standards, *Flow Meas. Instrum.* **11** (2000), pp. 329–337. Abstract | **Article** | PDF (419 K) | View Record in Scopus | Cited By in Scopus (8)

[13] M. Hayakawa, Y. Ina, Y. Yokoi, M. Takamoto and S. Nakao, Development of a transfer standard with sonic venturi nozzles for small mass flow rates of gases, *Flow Meas. Instrum.* **11** (2000), pp. 279–283. Abstract | **Article** | PDF (352 K) | View Record in Scopus | Cited By in Scopus (6)

[14] Japan Calibration Service System. http://www.iajapan.nite.go.jp/jcss/en/index.html.

[15] L.S. Rothman, I.E. Gordon, A. Barbe, D. Chris Benner, P.F. Bernath, M. Birk, V. Boudon, L.R. Brown, A. Campargue, J.-P. Champion, K. Chance, L.H. Coudert, V. Dana, V.M. Devi, S. Fally, J.-M. Flaud, R.R. Gamache, A. Goldman, D. Jacquemart, I. Kleiner, N. Lacome, W.J. Lafferty, J.-Y. Mandin, S.T. Massie, S.N. Mikhailenko, C.E. Miller, N. Moazzen-Ahmadi, O.V.

Naumenko, A.V. Nikitin, J. Orphal, V.I. Perevalov, A. Perrin, A. Predoi-Cross, C.P. Rinsland, M. Rotger, M. Šimečková, M.A.H. Smith, K. Sung, S.A. Tashkun, J. Tennyson, R.A. Toth, A.C. Vandaele and J. Vander Auwera, The HITRAN 2008 molecular spectroscopic database, *JQSRT* **110** (2009), pp. 533–572. Abstract | **Article** | PDF (1158 K) | View Record in Scopus | Cited By in Scopus (228)

[16] C. Delaye, J.-M. Hartmann and J. Taine, Calculated tabulations of H_2O line broadening by H_2O, N_2, O_2, and CO_2 at high temperature, *Appl. Opt.* **28** (1989), pp. 5080–5087.

[17] D. Lisak, D.K. Havey and J.T. Hodges, Spectroscopic line parameters of water vapor for rotation–vibration transitions near 7180 cm^{-1}, *Phys. Rev. A* **79** (2009), p. 052507. View Record in Scopus | Cited By in Scopus (2)

[18] ACS Committee on Environmental Improvement, Guidelines for data acquisition and data quality evaluation in environmental chemistry, *Anal. Chem.* **52** (1980), pp. 2242–2249.

[19] J.D. Winefordner and G.L. Long, Limit of detection: a closer look at IUPAC definition, *Anal. Chem.* **55** (1983), pp. 712A–724A.

[20] J.P. Looney, J.T. Hodges, R.D. van Zee, Quantitative absorption measurements using cavity-ringdown spectroscopy with pulsed lasers, in: K.A. Busch, M.A. Busch (Eds.), Cavity-Ringdown Spectroscopy: An Ultratrace-Absorption Measurement Technique, Oxford U. Press, Oxford, 1998, pp. 93–105 (Chapter 7).

[21] S.S. Brown, H. Stark, S.J. Ciiora, R.J. McLaughlin and A.R. Ravishankara, Simultaneous in situ detection of atmospheric NO_3 and N_2O_5 via cavity ring-down spectroscopy, *Rev. Sci. Instrum.* **73** (2002), pp. 3291–3301. View Record in Scopus | Cited By in Scopus (51)

[22] V. Vorsa, S. Dheandhanoo, S.N. Ketkar and J.T. Hodges, Quantitative absorption spectroscopy of residual water vapor in high-purity gases: pressure broadening of the 1.39253-μm H_2O transition by N_2, HCl, HBr, Cl_2, and O_2, *Appl. Opt.* **44** (2005), pp. 611–619. View Record in Scopus | Cited By in Scopus (4)

[23] J.B. Dudek, P.B. Tarsa, A. Velasquez, M. Wladyslawski, P. Rabinowitz and K.K. Lehmann, Trace moisture detection using continuous-wave cavity ring-down spectroscopy, *Anal. Chem.* **75** (2003), pp. 4599–4605. View Record in Scopus | Cited By in Scopus (35)

[24] M.A.H. Smith, C.P. Rinsland, B. Fridovich, K.N. Rao, Intensity and collision broadening parameters from infrared spectra, in: K. N. Rao (Ed.), Molecular Spectroscopy: Modern Research, vol. III, Academic Press, Orlando, 1985, pp. 111–248 (Chapter 3).

[25] B. Parvitte, V. Zéninari, I. Pouchet and G. Durry, Diode laser spectroscopy of H_2O in the 7165–7185 cm^{-1} range for atmospheric applications, *JQSRT* **75** (2002), pp. 493–505. Abstract | **Article** | PDF (201 K) | View Record in Scopus | Cited By in Scopus (21)

[26] J.T. Hodges, H.P. Layer, W.W. Miller and G.E. Scace, Frequency-stabilized single-mode cavity ring-down apparatus for high-resolution absorption spectroscopy, *Rev. Sci. Instrum.* **75** (2004), pp. 849–863. View Record in Scopus | Cited By in Scopus (36)

[27] J.T. Hodges and R. Ciuryło, Automated high-resolution frequency-stabilized cavity ring-down absorption spectrometer, *Rev. Sci. Instrum.* **76** (2005), p. 023112. View Record in Scopus | Cited By in Scopus (24)

Corresponding author.

Vitae

Hisashi Abe received his PhD degree in physics in 1996 from Kanazawa University, Japan. He is a senior researcher in the Humidity Standards Section of NMIJ.

Koichi M.T. Yamada, after obtaining the PhD in 1973 at the University of Tokyo, engaged in the high resolution molecular spectroscopy for 20 years in Germany as a DFG fellow at the University of Kiel, as an assistant professor of the University of Giessen, and of the University of Cologne. Since 1994, he had been a senior researcher at AIST, Japan, and after retirement in 2006 a guest researcher.

Sensors and Actuators A: Physical
Volume 165, Issue 2, February 2011, Pages 230-238

Sponsored Links

On Site Calibration Svcs
Best service at the best price
ISO9001, A2LA, cGMP, NIST traceable
www.integratedservicesolutions.com

Digital Oscilloscopes
Digital Oscilloscopes now from
Rohde&Schwarz. Get Details Here!
www.scope-of-the-art.com/RTO

Calibration by RAES
Nist traceable ANSI/MIL compliant.
Fast, free delivery in the USA
www.raelectrical.com

Copyright © 2011 Elsevier B.V. All rights reserved. SciVerse® is a registered trademark of Elsevier Properties S.A., used under license. ScienceDirect® is a registered trademark of Elsevier B.V.